Available online at www.sciencedirect.com
SCIENCE DIRECT
Applied Catalysis B: Environmental 56 (2005) 57–68
APPLIED CATALYSIS B: ENVIRONMENTAL
www.elsevier.com/locate/apcatb

Activity and stability of low-content gold–cerium oxide catalysts for the water–gas shift reaction

Qi Fu[1], Weiling Deng, Howard Saltsburg, Maria Flytzani-Stephanopoulos*

Department of Chemical and Biological Engineering, Tufts University, Medford, MA 02155, USA

Received 23 February 2004; received in revised form 7 July 2004; accepted 9 July 2004
Available online 12 October 2004

Abstract

We report here on the high activity and stability of low-content gold–cerium oxide catalysts for the water–gas shift reaction (WGS). These catalysts are reversible in cyclic reduction–oxidation treatment up to 400 °C, are non-pyrophoric, and are thus potential candidates for application to hydrogen generation for fuel cell power production. Low-content (0.2–0.9 at.%) gold–ceria samples were prepared by single-pot synthesis by the urea gelation/coprecipitation method; and by sodium cyanide leaching of high-content (2–8 at.%) gold–ceria materials prepared by various techniques. The low-content gold–ceria catalysts are free of metallic gold nanoparticles. Gold is present in oxidized form, as verified by a variety of analytical techniques. However, these materials display the same WGS activity as the high-content gold ones, and remain free of gold nanoparticles after use in a reaction gas stream composed of 11% CO–26% H_2O–26% H_2–7% CO_2–balance He up to 300 °C. We show that the determining factor for the retention of active gold in ceria is the surface properties of the latter. Measurements of lattice constant expansion indicate gold ion substitution in the ceria lattice. The turnover frequency of WGS under the assumption of fully dispersed gold is the same for a variety of low-content gold–ceria preparations. The stability of gold–ceria in various gas compositions and temperatures was good. The most serious stability issue is formation of cerium hydroxycarbonate in shutdown operation.

Keywords: Gold catalysts; Nanocrystalline cerium oxide; Water–gas shift reaction; Fuel cells; Cyanide leaching; Hydrogen generation; Stability of gold–ceria catalysts

1. Introduction

The water–gas shift (WGS) reaction is an integral part of fuel processing for the production of hydrogen. When hydrogen is used for fuel cell power generation, the WGS catalysts should be both active and stable in cyclic operation and in exposure to air and condensed water, and of course, economical. The state-of-the-art low-temperature WGS catalyst in chemical plants is Cu–ZnO [1]. However, this type catalyst is very sensitive to temperature excursions, pyrophoric if exposed to air, and requires very careful pre-activation. It has been assessed unsuitable for application to PEM fuel cells, especially for use in transportation. WGS catalysts based on nanocrystalline cerium oxide (ceria) have been investigated in recent years as alternatives to Cu–ZnO for fuel cell applications [2–6]. They are non-pyrophoric and can be used without activation [5]. It is well known that platinum metals (PM) supported on cerium oxide in the three-way automotive catalyst enhance the low-temperature WGS reaction and are much more active than PM/alumina [2,7]. Previous work in our laboratory has shown that Cu- and other transition metal-containing nanocrystalline cerias are active and stable catalysts in low- and high-temperature redox reactions [5,6,8–13]. Cu–ceria was found active for WGS over a wide temperature window [5]. The reducibility and catalytic activity of CeO_2 are significantly enhanced by the presence of a small amount of a transition metal, which does not have to be a platinum group metal. Platinum was the earliest case demonstrated of a metal additive having a considerable effect on ceria reducibility [14]. Among the

* Corresponding author. Tel.: +1 617 6273048; fax: +1 617 6273991.
E-mail address: mflytzan@tufts.edu (M. Flytzani-Stephanopoulos).
[1] Present address: Cabot Corporation, Albuquerque, NM, USA.

0926-3373/$ – see front matter © 2004 Elsevier B.V. All rights reserved.
doi:10.1016/j.apcatb.2004.07.015

metal–ceria systems examined in the literature, Au–ceria is a particularly active and stable catalyst for low-temperature CO oxidation [10,11,15], methane oxidation [10,11], and the WGS reaction [6,12,13,16].

The literature of fine gold particles supported on reducible oxides has focused on the gold particle size and properties [17–19]. However, it is possible that the oxide support is much more important than given credit to date [6,12,13,16]. Little is known about the interaction of Au with ceria that might be responsible for the observed high activity. We recently reported that nonmetallic gold and platinum species on ceria are associated with the active sites for the water–gas shift reaction [6]. In the present work, we further examine the gold–ceria interaction and evaluate the catalyst under realistic operating conditions.

2. Experimental

2.1. Catalyst preparation and characterization

Lanthana- or gadolinia-doped ceria and undoped ceria materials were prepared by the urea gelation/coprecipitation (UGC) method [5]. Gold–ceria samples were prepared by deposition precipitation (DP), coprecipitation (CP) and the above UGC method [5], as described in detail elsewhere [12].

Leaching of gold from calcined gold–ceria samples took place in an aqueous solution of 2% NaCN under O_2 gas sparging at room temperature. Sodium hydroxide was added to keep the pH at ~12. Cyanide leaching is a very fast process. The remaining amount of gold is almost the same after 1 or 24 h. This is a well-known process used to extract gold during gold mining [20]. The leaching process is also very selective. No cerium or lanthanum was found in the leachate, as examined by ICP. No sodium was found in the leached samples, as examined by ICP and XPS. Cyanide leaching removed ~90% of the gold from the parent gold–ceria samples. After leaching, the color of gold–ceria catalysts changed from dark blue to greenish yellow. The leachate solution was colorless. Leached samples were washed by deionized water three times; then dried in a vacuum oven for 10 h, and heated in air at 400 °C for 2 h.

All reagents used in catalyst preparation were analytical grade. The samples reported here are denoted as *a*Au–CL or CG (z), where *a* is the gold content in atomic percent, $100 \times (\mathrm{Au/MW_{Au}})/(\mathrm{Au/MW_{Au}} + \mathrm{Ce/MW_{Ce}} + \mathrm{La\ or\ Gd/MW_{La\ or\ Gd}})$; CL is 10 at.% La-doped ceria, CG is 10 or 30 at.% Gd-doped ceria; z is the method of preparation: CP, DP or UGC. The calcination temperature was typically 400 °C. The calcination temperature, *T*, of the ceria support used to prepare DP samples is also included in the parentheses, e.g. *a*Au–CL (DP, T). T was typically 400 or 650 °C.

The BET surface area was measured by single-point N_2 adsorption/desorption cycles in a Micromeritics Pulse ChemiSorb 2705 flow apparatus. Bulk composition analysis of the catalyst was conducted in an inductively coupled plasma optical emission spectrometer (ICP-OES, Leeman Labs Inc.).

XRD analysis was performed in a Rigaku 300 instrument with a rotating anode generator and a monochromatic detector. Cu $K\alpha_1$ radiation was used with a power setting of 60 kV and 300 mA. The mean crystallite size was determined according to the Scherrer equation [21] and the lattice parameter, α, was calculated from ceria $\langle 1\ 1\ 1 \rangle$ or $\langle 2\ 2\ 0 \rangle$ reflections by the equation:

$$\alpha = \sqrt{h^2 + k^2 + l^2}\left(\frac{\lambda}{2\,sin\,\theta}\right)$$

The software TOPAS (Bruker) was used to perform profile fitting, lattice parameter refinement and microstructure analysis.

A Kratos AXIS Ultra Imaging X-ray Photoelectron Spectrometer with a resolution of 0.1 eV was used to determine the atomic metal ratios of the surface region and the metal oxidation state of selected catalysts. Samples were in powder form and were pressed on a double-side adhesive copper tape. All measurements were carried out at room temperature without any sample pre-treatment. An Al Kα X-ray source was used in this work. All binding energies were adjusted to the C 1s peaks at 285 eV. An adjacent neutralizer was used to minimize the static charge on the samples.

Scanning transmission electron microscopy (STEM) analyses were performed in a Vacuum Generators HB603 STEM equipped with a X-ray microprobe of 0.14 nm optimum resolution for energy dispersive X-ray spectroscopy (EDX). The sample powder was dispersed on a copper grid coated with a carbon film and elemental maps were obtained on a 128 × 128 data matrix.

High-resolution transmission electron microscopy (HRTEM) analyses were performed on a JEOL 2010 instrument, operating at 200 kV with a lanthanum hexaboride cathode. The sample powder was suspended in isopropyl alcohol using an ultrasonic bath and deposited on a carbon coated 200 mesh Cu grid.

2.2. Apparatus and experimental procedures

Temperature-programmed reduction by hydrogen (H_2-TPR) and carbon monoxide (CO-TPR) was conducted in a Micromeritics Pulse ChemiSorb 2705 instrument equipped with a thermal conductivity detector and coupled with an on-line residual gas analyzer (MKS-model RS-1) to detect CO, CO_2, H_2, H_2O and O_2.

The as-prepared catalysts in fine powder form were first oxidized in a 20% O_2/He gas mixture (50 cm^3/min (NTP)) at 350 °C for 30 min, cooled down to room temperature and then purged with pure helium (Grade 5). The sample was then heated at a rate of 5 °C/min from room temperature to 900 °C in a 20% H_2/N_2 or 10 % CO/He gas mixture (50 cm^3/

min (NTP)). The CO/He gas stream passed through a hydrocarbon trap (Alltech) to remove any traces of hydrocarbons from the mixture. In cyclic CO-TPR experiments, heating was stopped at 400 °C, and was followed by exposure of the catalyst to a 20% O_2/He gas mixture (50 cm^3/min (NTP)) at 350 °C. The subsequent cooling and heating process was as described above.

WGS reaction tests and kinetics measurements were conducted at atmospheric pressure with the catalyst in powder form (<150 μm). A quartz tube (OD = 1 or 0.5 cm) with a porous quartz frit supporting the catalyst was used as a packed-bed flow reactor. All samples were used in the as prepared form without activation. Water was injected into the flowing gas stream by a calibrated syringe pump and vaporized in the heated gas feed line before entering the reactor. A condenser filled with ice was installed at the reactor exit to collect water. The feed and product gas streams were analyzed by a HP-6890 gas chromatograph (GC) equipped with a thermal conductivity detector (TCD). A Carbosphere (Alltech) packed column (1.8 m × 0.318 cm) was used to separate H_2, CO, CH_4 and CO_2.

The production rate of CO_2 was used to calculate the reaction rate:

$$\text{rate}\,(\text{mol/g s}) = \frac{N_t^{out} \times CO_2^{out} - N_t^{in} \times CO_2^{in}}{W_{cat}}$$

where N_t^{in} or N_t^{out} is the total molar flow rate in mol/s of feed or product gas stream at dry condition, CO_2^{in} or CO_2^{out} is the molar fraction of CO_2 in the feed or product gas stream at dry condition, and W_{cat} is the catalyst weight in grams. Since N_t^{out} cannot be monitored continuously, N_t^{out} is expressed as $N_t^{in}(CO_2^{in} + CO^{in})/(CO_2^{out} + CO^{out})$, where N_t^{in} was measured before reaction and the concentration of CO and CO_2 were measured by GC. The rate based on CO consumption was equal to the rate of CO_2 production. No methane was produced under any of the reaction conditions used in this work.

3. Results and discussion

3.1. Fresh catalyst characterization

Table 1 shows the physical properties of doped and undoped ceria prepared by UGC; and the properties of gold-containing cerias. Doping of ceria with La_2O_3 was used in our previous work to stabilize the crystal growth of ceria [9,12,13]. Here we show that doping ceria with gadolinia, Gd_2O_3, is equally effective. The ionic radii of both La^{3+} (0.116 nm) and Gd^{3+} (0.105 nm) are bigger than Ce^{4+} (0.097 nm) [7]. Their substitution in the ceria lattice increases the lattice constant α, as is clearly shown in Table 1. Of course, for charge neutrality, oxygen ion vacancies (one per two trivalent cations substituted) are created in the thus doped ceria.

The physical properties of the as prepared and leached samples are compared in Table 1. The surface areas, crystallite sizes of ceria, and lattice constants all remained almost the same after leaching and heat treating the samples at the same conditions as the parent materials. The amount of residual gold in the leached gold–ceria samples was less than 1 at.%, and was about 10% of the original amount of gold in the parent samples. Low-content gold–ceria and doped ceria samples were also prepared by one-pot synthesis by the UGC method. The properties of these materials are also shown in Table 1.

The structure of the as-prepared and leached gold–ceria samples was examined by STEM/EDX. Fig. 1 shows typical O, Au and Ce elemental maps obtained by X-ray microprobe for DP- and CP-prepared parent samples (Fig. 1a and c) and the corresponding leached samples (Fig. 1b and d). From the images, we can see that the distributions of O and Ce in the elemental maps are very similar, suggesting that Ce and O are closely associated. In as prepared, high-content gold–ceria materials [12], well-rounded gold nanoparticles in contact with ceria are the dominant structure. In the leached materials, gold is no longer present as individual particles. The residual gold appears to be atomically dispersed in the ceria matrix.

X-ray diffraction data were collected for undoped CeO_2, La- or Gd-doped ceria and as prepared and leached gold–ceria materials. XRD patterns of selected materials are shown in Fig. 2. All patterns have distinct crystal phases of fluorite oxide-type CeO_2. A small broad peak corresponding to Au(1 1 1), and a barely visible peak corresponding to Au(2 0 0), are seen in two of the samples containing more than 3 at.% Au. Gold is non-detectable in the leached samples. From XRD analyses, lattice constants were calculated, as were the crystallite sizes of gold and ceria by the Scherrer equation. These are included in Table 1. As reported before [12,13], the preparation method affects the properties of gold–ceria. This is seen in Table 1 for the Au–CL samples prepared by UGC, DP, and CP; namely, the parent samples 8Au–Cl, 4.7Au–CL, and 4.4Au–CL, and their respective leached derivatives. The UGC method is superior to CP as shown by the smaller particle size of the resulting ceria after similar heat treatment. Thus, gold suppresses the particle growth of ceria in the UGC preparation.

If Au^{3+} ions (0.099 nm radius [21]) substitute into the ceria lattice, this should be accompanied by an increase of the value of the lattice constant. The lattice constants of the Au–CL samples prepared by UGC are higher than those of the corresponding Au-free CL material, indicative of gold ion substitution in the ceria lattice. Thus, while 8Au–CL(UGC) contains large metallic gold particles, it also has some of its gold in oxidized form, bound to ceria. This is also corroborated by the similar values of the lattice constant of the corresponding leached sample, 0.9Au–CL. Comparison of the lattice constants of 0.94Au–CeO_2(UGC) to CeO_2(UGC) more clearly shows gold ion substitution in

Table 1
Physical properties of ceria-based catalysts[a]

Sample	BET surface area (m^2/g)	Surface Au content[b] (at.%)	Bulk composition[c] (%)			Crystallite size[d] (nm)			Lattice constant[e] (Å)	
			Au	Ce	La or Gd	Au	CeO_2		CeO_2	
						⟨1 1 1⟩	⟨1 1 1⟩	⟨2 2 0⟩	⟨1 1 1⟩	⟨2 2 0⟩
8Au–CL(UGC)	158.1	2.32	8.11	83.99	7.90	49.1, 36.6[f]	4.5	4.5	5.459	5.434
0.9Au–CL(UGC, NaCN)	150.6	1.01	0.90	91.66	7.44	0	4.5	4.5	5.470	5.440
4.7Au–CL(DP)	156.1	1.60	4.71	87.88	7.41	5.0	5.2	4.9	5.431	5.428
0.44Au–CL(DP, NaCN)	157.9	0.61	0.44	91.24	8.32	ND	5.2	4.9	5.438	5.443
4.4Au–CL(CP)	47.8	3.29	4.35	88.00	7.65	12.9	7.2	6.3	5.472	5.448
0.7Au–CL(CP, NaCN)	47.5	0.24	0.67	91.52	7.82	ND	7.0	6.0	5.464	5.435
2.8Au–CL(DP)	159.2	1.58	2.81	89.16	8.03	4.7	5.0	4.9	NM	NM
0.23Au–CL(DP, NaCN)	162.2	0.43	0.23	93.10	6.67	ND	5.0	4.9	NM	NM
3.4Au-CeO_2(DP)[g]	25.9	NM	3.36	96.64	0	4.0	21.1	20.3	5.404	5.404
0.001Au–CeO_2(DP, NaCN)[g]	28.0	NM	∼0.001	∼99.999	0	ND	21.0	20.4	5.406	5.407
2.4Au–CG(DP)	170.6	1.63	2.40	67.10	30.50	3.1	4.6	5.3	5.418	5.433
0.54Au–CG(DP, NaCN)	184.6	0.50	0.54	68.96	30.50	ND	4.5	5.4	5.413	5.427
0.69Au–CeO_2(UGC)	170.1	NM	0.69	99.31	0	ND	5.0	6.2	5.418	5.417
0.94Au–CeO_2(UGC)	180.5	NM	0.94	99.06	0	ND	4.3	5.4	5.440	5.430
0.56Au–CG(UGC)	160.6	NM	0.56	88.6	10.84	ND	5.1	6.4	5.423	5.425
CG(UGC)	173.2	–	0	89.81	10.19	–	5.0	6.3	5.465	5.448
CeO_2(UGC)	140.5	–	0	100	0	–	7.1	6.6	5.415	5.416
CeO_2(UGC)[h]	75.0	–	0	100	0	–	9.9	9.8	5.412	5.411
CeO_2(UGC)[g]	25.9	–	0	100	0	–	21.1	20.3	5.411	5.409
CL(UGC)	156.9	–	0	92.62	7.38	–	5.1	4.8	5.438	5.442
CL(CP)	72.2	–	0	NM	NM	–	7.4	7.0	NM	NM

[a] All samples calcined at 400 °C for 10 h, except leached samples for 2 h; CL: Ce(10% La)O_x; CG: Ce(10 or 30% Gd)O_x calcined at 400 °C, 10 h; NM: not measured; ND: non-detectable.
[b] The surface metal ratio was determined by XPS.
[c] Bulk composition was determined by inductively coupled plasma (ICP).
[d] The crystallite size was determined by XRD with the Scherrer equation.
[e] The lattice constant was determined by the expression $\alpha = \sqrt{h^2 + k^2 + l^2}(\lambda/2\sin\theta)$
[f] Au ⟨2 0 0⟩.
[g] CeO_2 was calcined at 800 °C, 4 h.
[h] Calcined at 650 °C, 4 h.

ceria, because the effect is not masked by the presence of other dopants (La, Gd). The corresponding particle size of gold-doped ceria is considerably smaller than that of gold-free ceria. Gold ion substitution in the ceria lattice is inferred also in samples prepared by CP. The DP-prepared samples show the smallest effect; this may be attributed to the method of preparation and to the lower amount of residual gold in the leached samples. Lattice constant increase can also be due to Ce^{3+} formation as the crystal size of ceria decreases [22]. Further analysis is needed to properly attribute the observed increase of α to Au^{3+}, Ce^{3+} or both.

By leaching again the leached material 0.7Au–CL(CP, NaCN), which had been calcined at 400 °C for 2 h, we found that no gold was removed this time. This shows that gold did not segregate to form gold clusters or particles in the calcination step. Thus, a strong association between gold and ceria is inferred which stabilizes the gold ions in the ceria matrix. The surface gold content and the oxidation states of Au in both the parent and leached ceria samples were checked by XPS. The surface gold contents of the parent DP, CP and UGC samples are grossly underestimated (Table 1), because the average gold crystallite sizes greatly exceed the electron escape depth. However, the agreement is better for the leached Au–ceria samples. Au^0, Au^{1+}, and Au^{3+} oxidation states were identified in the parent gold–ceria samples by XPS [6,13], while the leached samples contained only ionic gold [6].

Fig. 3 shows H_2-TPR data collected over a DP-prepared gold–ceria, 2.4AuCG-DP, and its corresponding NaCN-leached sample, 0.54Au–CG. Consumption of hydrogen is similar for both the parent and leached samples. However, reduction of the latter is shifted to higher temperatures, indicating the presence of more strongly bound ionic gold.

3.2. Activity of low-content gold–ceria catalysts

Similar WGS reaction rates of CO_2 production (per square meter of catalyst surface area) were measured over the parent (8Au–CL(UGC), 4.4Au–CL(CP) and 4.7Au–CL(DP)) and the respective leached (0.9Au–CL(UGC, NaCN), 0.7Au–CL(CP, NaCN) and 0.44Au–CL(DP, NaCN) catalysts. For instance, at 300 °C, the WGS rate on 8Au–CL(UGC) is 0.14 μmol CO_2/m^2 s, that over 4.4Au–CL(CP) is 0.18 μmol CO_2/m^2 s and that over 4.7Au–CL(DP) is 0.07 μmol CO_2/m^2 s. By comparison, the WGS rate on the leached sample 0.9Au–CL(UGC, NaCN) is 0.13 μmol CO_2/m^2 s, that

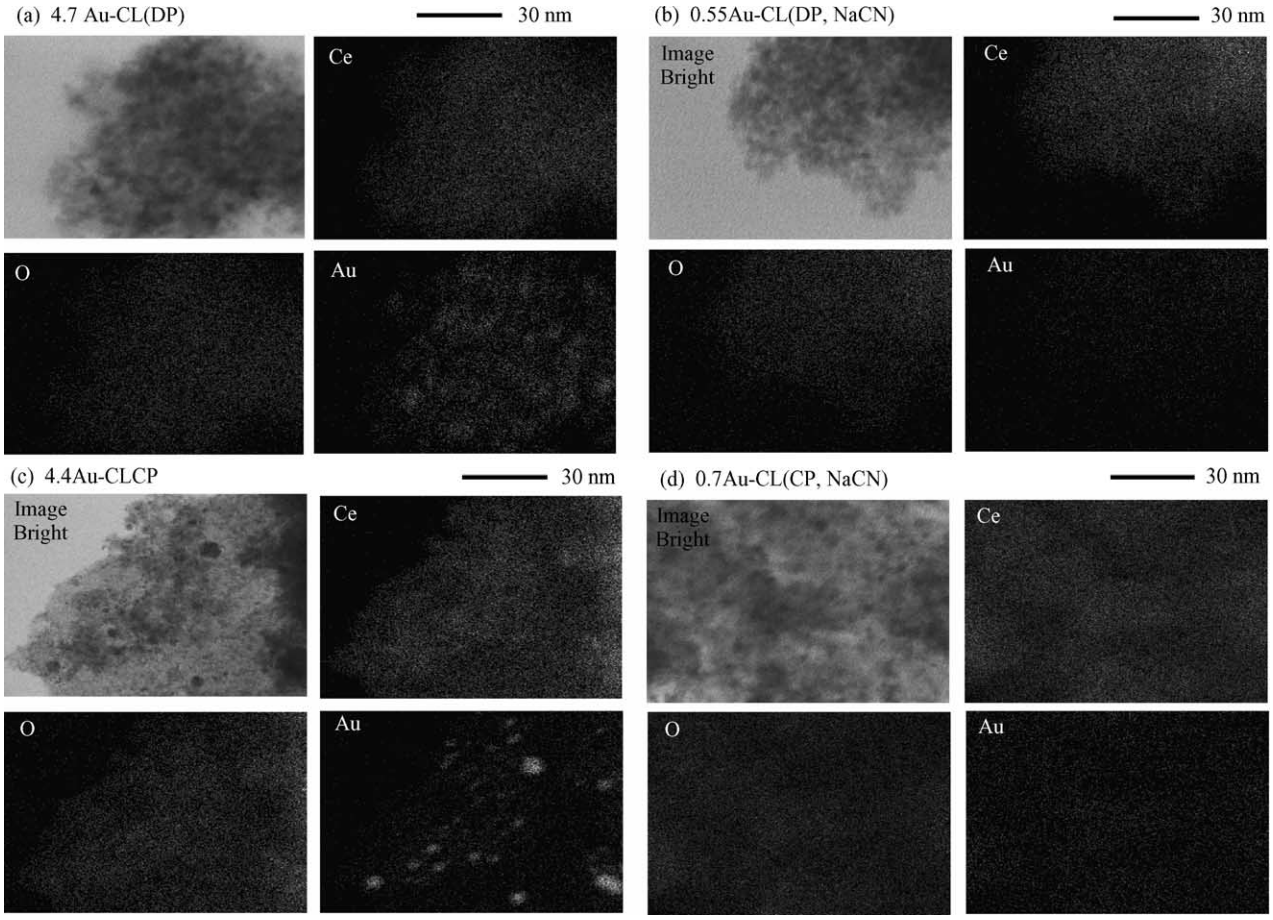

Fig. 1. STEM/EDX of as prepared and leached gold–ceria samples (see Table 1 for properties). Gold particles are removed by NaCN leaching.

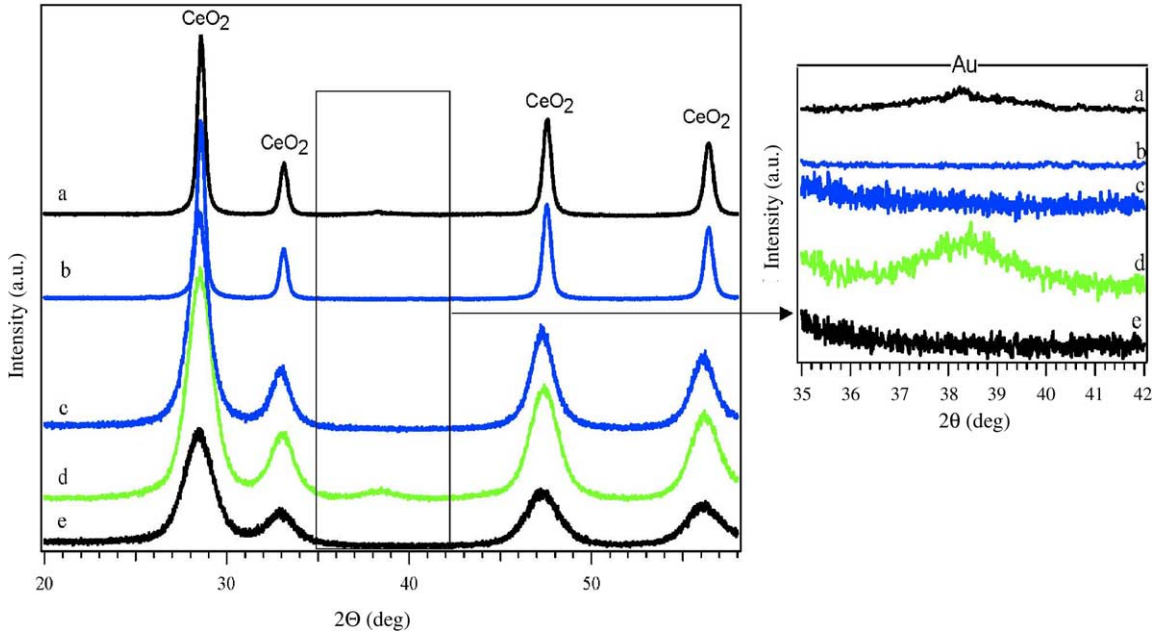

Fig. 2. XRD patterns of as prepared and leached gold–ceria samples (see Table 1 for properties): (a) 3.4Au–CeO_2 (800 °C) (DP); (b) 0.001Au–CeO_2 (800 °C) (DP, NaCN); (c) 0.7Au–CL(CP, NaCN); (d) 4.7Au–CL(DP); (e) 0.44Au–CLDP, NaCN).

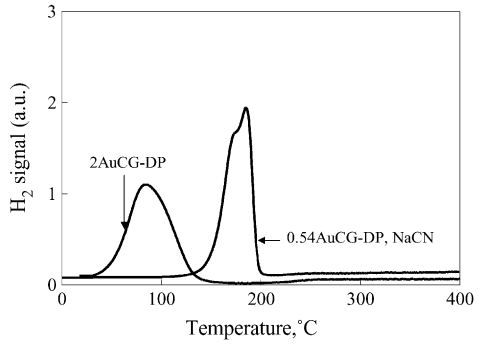

Fig. 3. H_2-TPR profiles of 2.4% Au–Ce (30% Gd)O_x prepared by deposition–precipitation and its NaCN-leached derivative, 0.54% Au–Ce (30% Gd)O_x. Test condition: 20% H_2/N_2, 50 cm^3/min (STP); 5 °C/min. Catalysts were pretreated in 20% O_2/He at 350 °C for 30 min.

over 0.7Au–CL(CP, NaCN) is 0.16 μmol CO_2/m^2 s and that over 0.44Au–CL(DP, NaCN) is 0.10 μmol CO_2/m^2 s. The apparent activation energy of the reaction was the same for parent and leached catalyst samples, 47.0 ± 2.7 kJ/mol for UGC samples, 47.8 ± 1.5 kJ/mol for the DP samples and 36.8 ± 0.9 kJ/mol for the CP samples. Therefore, from the activity tests, we can conclude that metal gold nanoparticles do not participate in the water–gas shift reaction.

On the basis of the STEM/EDX, XRD, XPS, and H_2-TPR data discussed above, the active site for the WGS reaction appears to be a Au–O–Ce phase, involving ionic gold bound strongly in the ceria surface and subsurface layers. These sites are present in both the parent and leached catalysts; their number is "titrated" by cyanide leaching, which removes all the weakly bound gold from the ceria surface. It is of interest, therefore, to assume atomic dispersion of gold in the leached samples and cast the steady-state reaction rates in terms of a turnover frequency (TOF) Arrhenius-type plot. Fig. 4 shows such a plot, constructed from the rates of CO_2 molecules produced/s/Au–O–Ce site over the low-content gold–ceria catalysts examined in this work. Data from the leached samples as well as from samples prepared

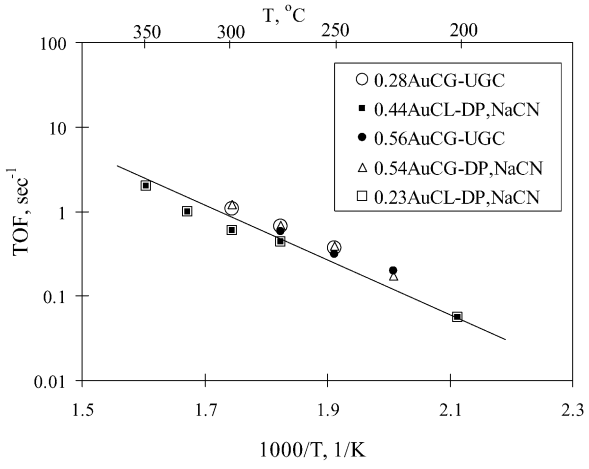

Fig. 4. Turnover frequency plot for the WGS reaction over low-content gold–ceria catalysts in 11% CO–26% H_2O–26% H_2–7% CO_2–He.

by single-pot UGC with low-content gold are included in Fig. 4. The agreement of the WGS reaction TOFs over samples prepared by such different methods and of such different compositions is remarkable.

The residual gold amount after leaching must be related to the surface properties of ceria. Only a strong association with the surface Ce–OH groups would keep the gold from dissolving in the cyanide solutions. Undoped ceria samples prepared by UGC were calcined at 400, 650 and 800 °C, to change their surface areas (Table 1). The material calcined at 400 °C has a surface area of 140.5 m^2/g with an average crystallite size of cerium oxide of 6.9 nm. The surface area of the material calcined at 650 °C is 75 m^2/g with an average ceria crystallite size of 10 nm, while that of the material calcined at 800 °C is 25.9 m^2/g with an average crystallite size of ∼20 nm. The concentration of oxygen surface defects decreases with the cerium oxide particle size for nanoparticles of ceria of size <20 nm [22]. Gold (6.3, 4.1, and 3.4 at.%) was deposited on the 400, 650, and 800 °C-ceria samples, respectively, by the DP method. The catalysts were then calcined in air at 400 °C, 2 h. NaCN leaching of these samples had the following effect: the amount of gold remaining after leaching decreased with the particle size of ceria. These results are shown in Fig. 5. Thus, the cerium oxide material with the smallest particle size or with the highest number of oxygen defects retains the highest amount of gold after leaching.

In order for the ceria–gold interaction to commence, the DP-prepared samples must be heated in air to ∼200 °C or higher. We proved this by leaching samples immediately after gold deposition, but before heating, which failed to produce an active catalyst. Therefore, diffusion of Au ions into ceria takes place during the heating step in the preparation process. Interestingly, thermal treatment in the reformate-type gas mixture of 11% CO–7% CO_2–26% H_2–26% H_2O–He sets off the diffusion of Au ions at lower temperatures. After heating in this reformate gas mixture up to 225 °C, a part of Au is non-leachable. During the heating step, oxidized gold species mostly decompose into neutral species, diffusing to form metallic particles. Thus, only a small part of gold ends up as active Au–O–Ce species.

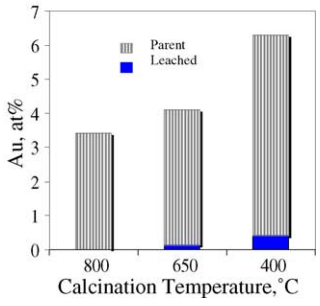

Fig. 5. Gold amount before and after leaching vs. ceria prepared with different particle size at 800, 650 and 400 °C. Parent catalysts: 3.4, 4.1 and 6.3% Au–CeO_2 made by DP; leached catalysts: 0, 0.16 and 0.44 at.% Au–CeO_2, respectively.

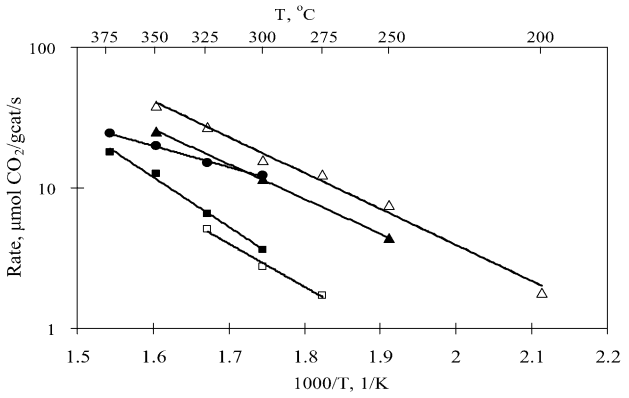

Fig. 6. Steady-state WGS reaction rates measured in 11% CO–26% H_2O–26% H_2–7% CO_2–He. Solid triangles: 4.7Au–CL(DP); open triangles: leached 0.44Au–CL(DP, NaCN); solid circles: 0.62Au–TiO_2(DP), reference catalyst type A from World Gold Council; solid squares: 2.02Au–Fe_2O_3(CP), reference catalyst type C from World Gold Council; open squares: leached 0.73Au–Fe_2O_3(CP, NaCN).

The identification of Au ions [6], along with the increased amount of surface oxygen in the leached samples, Ref. [6] and Fig. 3, argues in favor of lattice substitution. Annealing of ceria effectively reduces the number of its oxygen defects. As can be seen in Table 1 and Fig. 5, large-sized, 800 °C-treated ceria particles do not retain gold after leaching, and are inactive at low temperatures. Hence, oxide surfaces with a high number density of oxygen defects are needed to prepare an active catalyst.

The WGS reaction activity of gold–ceria was compared to reference gold catalysts purchased from the World Gold Council. Fig. 6 shows Arrhenius-type plots for the steady-state WGS reaction rates over the 4.7Au–CL(DP) sample; its leached derivative, 0.44 Au–CL(NaCN); two gold reference catalysts, type A (1.5 wt.% Au/TiO_2, prepared by DP) and type C (5.0 wt.% Au/Fe_2O_3, prepared by coprecipitation). The gold loading is expressed in at.% in all samples shown in Fig. 6. Also shown in Fig. 6 is the rate measured over type C catalyst after leaching it in NaCN solution. Notably, the leached form of this reference catalyst, after removal of approximately two thirds of its gold loading by NaCN, was of comparable activity to its parent. Hence, iron oxide also binds gold strongly, similar to ceria. On the other hand, type A sample lost all of its gold and all its activity after leaching. We attribute this to the method of preparation and the low-surface area of the titania support.

3.3. Stability of gold–ceria catalysts

3.3.1. Annealing in air

We have found in previous work that certain dopants, such as lanthana, stabilize ceria and prevent its sintering [9,12]. As can be seen in Table 2, the surface area of CeO_2 calcined at 800 °C is only 25.9 m^2/g if undoped, while that of La-doped ceria is 43.6 m^2/g. Remarkably, the surface area of leached Au–ceria, which contains only 0.44% Au, is 61.1 m^2/g, after the 800 °C thermal treatment. Re-leaching the 800 °C-treated sample reduced the Au amount from 0.44 to 0.14%. In another case, further annealing of 4.7Au–CL(DP) at 800 °C for 4 h, decreased its surface area from 156.1 to 44.3 m^2/g. Leaching this sample by NaCN reduced the gold content to 0.2% and increased the surface area to 61.3 m^2/g. Thus, not only is gold stabilized in the ceria matrix, but also the embedded Au suppresses the sintering of ceria.

3.3.2. Stability in WGS reaction conditions

Catalyst stability evaluation is important both to improve our fundamental understanding of the activity, and to enable practical catalyst designs. Zalc et al. [23] reported a rapid first-order deactivation of Pt–ceria catalysts under reaction conditions and attributed it to over-reduction of ceria; further claiming that ceria-based catalysts are not suitable for WGS in fuel processing. Similar deactivation of Pt–CeO_2 catalysts was reported by Ghenciu [24]. Wang et al. [25] conducted accelerated aging of Pd/ceria in different gas mixtures. They found that only aging the catalyst in CO gas led to deactivation and argued that deactivation is induced by metal particles agglomeration in the presence of CO, which can be avoided by proper catalyst design to improve the metal-support interaction that stabilizes the palladium metal particles.

The stability of gold–ceria catalysts under WGS conditions has not been adequately addressed in the literature. Kim and Thompson [26] observed a fast and considerable (∼50%) loss of activity in their gold–ceria catalyst, which was initially more active than a high activity

Table 2
Physical properties of Au–ceria after different thermal treatments

Sample	Support calculated temperature (°C)	Catalyst calculated temperature (°C)	BET surface area (m^2/g)
CeO_2 (UGC)	800 °C, 4 h		25.9
Ce(La)O_2 (UGC)	800 °C, 4 h		43.6
0.44 Au–CL(DP, NaCN)	400 °C, 10 h	400 °C, 2 h	157.9
0.44Au–CL(DP, NaCN)	400 °C, 10 h	800 °C, 4 h	61.1
0.14Au–CL(DP, NaCN)[a]		400 °C, 2 h	61.5
4.7Au–CL(DP)	400 °C, 10 h	400 °C, 10 h	156.1
4.7Au–CL(DP)	400 °C, 10 h	800 °C, 4 h	44.3
0.2Au–CL(DP, NaCN)[b]		400 °C, 2 h	61.3

[a] Re-leached with NaCN from 0.44Au–CL(DP, NaCN) (properties shown in the row, immediately above), which was heated at 800 °C, 4 h.
[b] Leached from the parent catalyst 4.7Au–CL(DP) (properties shown in the row, immediately above), which was heated at 800 °C for 4 h.

Table 3
Surface area and ceria particle size changes after WGS reaction[a]

Sample	Surface area (m^2/g)		Particle size[b] (nm)					
	Fresh	Used	Fresh			Used		
			Au ⟨1 1 1⟩	CeO_2 ⟨1 1 1⟩	CeO_2 ⟨2 2 0⟩	Au ⟨1 1 1⟩	CeO_2 ⟨1 1 1⟩	CeO_2 ⟨2 2 0⟩
4.7Au–CL(DP)	156.1	131.1[c]	5.0	5.2	4.9	7.2[c]	5.7[c]	4.7[c]
		128.4[d]				6.2[d]	5.3[d]	4.9[d]
0.44Au–CL(DP, NaCN)	157.9	129.9[c]	ND	5.2	4.9	ND[c]	6.4[c]	6.2[c]
						ND[e]	5.4[e]	5.2[e]
4.7Au–CL(DP, 650)	82.7	71.6[f]	4.6	7.1	6.9	6.8[f]	7.3[f]	7.2[f]
3.8Au–CL(CP)	71.8	61.3[f]	6.7	5.8	5.3	7.2[f]	7.0[f]	6.4[f]
8Au–CL(UGC)	158.1	118.7[c]	49.1, 36.6[g]	4.5	4.5	65.1[c], 59.4[cg]	5.0[c]	4.8[c]

[a] All catalysts are as prepared and calcined at 400 °C; ND: non-detectable; NM: not measured.
[b] Determined by XRD, using the Scherrer equation.
[c] Used in 5% CO–15% H_2O–35% H_2–He for 100 h; space velocity 15,000 h^{-1}; reaction temperature: 250 °C.
[d] Used in 2% CO–10% H_2O–He for 70 h, space velocity 80,000 h^{-1}; temperature range: 150–350 °C.
[e] Used in 11% CO–26% H_2O–7% CO_2–26% H_2–He for 100 h, temperature: 300 °C.
[f] Used in 7% CO–38% H_2O–11% CO_2–40% H_2–He for 120 h, temperature range: 150–350 °C.
[g] Au ⟨2 0 0⟩.

commercial Cu–Zn–Al catalyst. They attributed this to loss of active sites by either carbonates or hydrocarbons formed during the WGS reaction. In the present work, we conducted different tests to check the stability of Au–ceria over a wide range of temperatures and different WGS gas compositions. In a 120 h long stability test of the 4.7Au–CL(DP, 650) sample (Table 3) at 300 °C, the catalytic activity remained almost the same in a reformate-type gas mixture containing 7% CO–38% H_2O–11% CO_2–40% H_2–He (space velocity 6000 h^{-1} (NTP)). No significant changes were observed in the conversion of CO (around 60%) during this period. Catalyst characterization after this test, found that the ceria crystallite size had increased only slightly, while the gold crystallite size grew by 47% to 6.8 nm (Table 3). The total surface area had changed from 82.7 to 71.6 m^2/g cat.

Three catalyst samples: 8Au–CL(UGC), 4.7Au–CL(DP), and 0.44Au–CL(DP, NaCN), were tested in a gas mixture containing 5% CO–15% H_2O–35% H_2–He, at 250 °C and at a space velocity of 15,000 h^{-1} (NTP) for 100 h. The CO conversion vs. time plot is shown in Fig. 7. The conversion dropped ~20% in the first 10 h and was then stabilized with very slow further decay. The surface area of both the parent and the leached DP-samples after 100 h on-stream were similar, ~130 m^2/g cat.

Table 3 shows the surface areas and crystallite sizes of gold and ceria in the as prepared and used Au–CL samples. Growth of crystallite size of gold and ceria is seen in the used catalysts. As discussed above, the gold crystallite size has little effect on the catalytic activity. Therefore, the initial activity loss is not due to the growth of gold particles. However, it is possible that the growth of ceria crystallite size weakens the interaction of Au and ceria. The surface area dropped 20 ± 5%, after use in various reaction gas mixture and temperatures. The surface area loss is in agreement with the long-term activity loss shown in Fig. 7. From these results, we may attribute the initial activity loss to surface area loss of ceria as a result of exposure of the catalyst to the WGS reaction mixture.

The oxidation state of gold may be affected by the reactant gas composition. Recently, Guzman and Gates [27] prepared cationic gold on MgO crystals and reported that Au^{3+} is reduced to Au^{1+} and subsequently Au^0 in reducing atmospheres even at room temperature. Au^{1+} and Au^0 were formed and Au^{3+} disappeared after exposure of the supported Au^{3+} complex to a mixture of CO and O_2.

In the present work, we found cationic Au in all gold–ceria samples prepared by various techniques, and after use in the WGS environment for many hours. XPS analysis of Au–ceria catalysts after 15 h use in the reaction gas mixture of 11% CO–26% H_2O–7% CO_2–26% H_2–He (at the

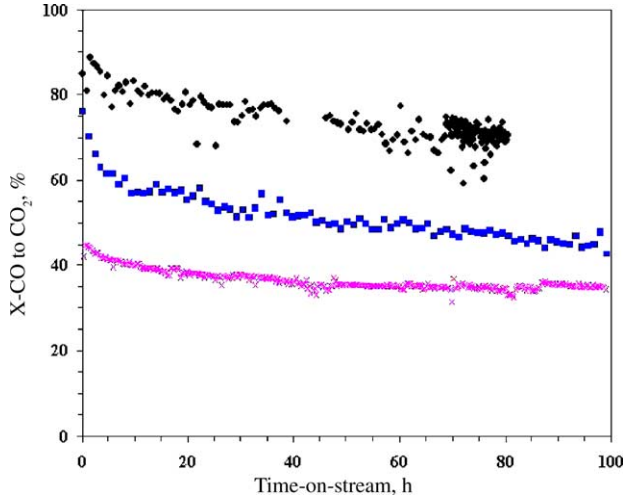

Fig. 7. Stability of gold-ceria WGS catalysts (see Table 1 for properties). Space velocity: 15,000 h^{-1} (NTP); 5% CO–15% H_2O–35% H_2–He; reaction temperature: 250 °C. Diamonds: 8Au–CL(UGC); crosses: 4.7Au–CL(DP); squares: 0.44Au–CL(DP, NaCN); all catalysts calcined at 400 °C (see Table 1 for properties).

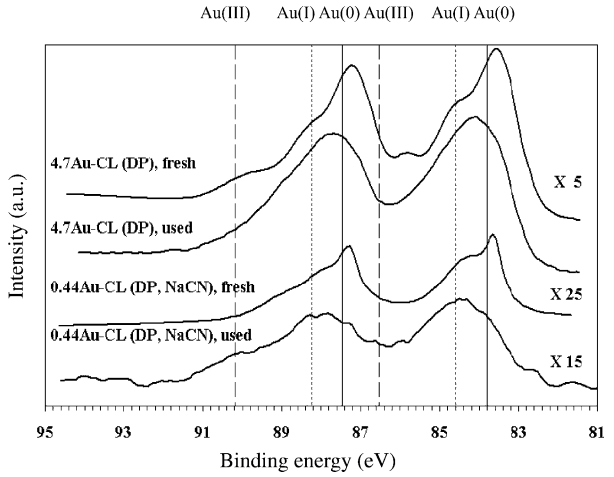

Fig. 8. XP spectra of fresh and used Au–ceria samples (see Tables 1 and 3 for properties).

conditions of Fig. 4) shows predominance of ionic Au, Fig. 8. This is true for both the parent and the NaCN-leached catalysts. It is also significant that the used leached catalyst, after more than 20 h in the above reaction gas mixture, could not be further leached. This suggests that gold is stabilized in the ceria matrix.

However, in the absence of in situ identification, it is plausible to question whether during reaction under net reducing conditions, zerovalent gold may be formed. Gradually, gold migration and agglomeration into metallic particles could take place. Therefore, we characterized our catalysts by XPS after use in WGS under various reaction conditions to examine the oxidation state of gold. Samples were exposed to air before the XPS analysis. The XP spectra of 4.7Au–CL(DP) as prepared and after use in various WGS gas mixtures are shown in Fig. 9. The oxidation state of gold

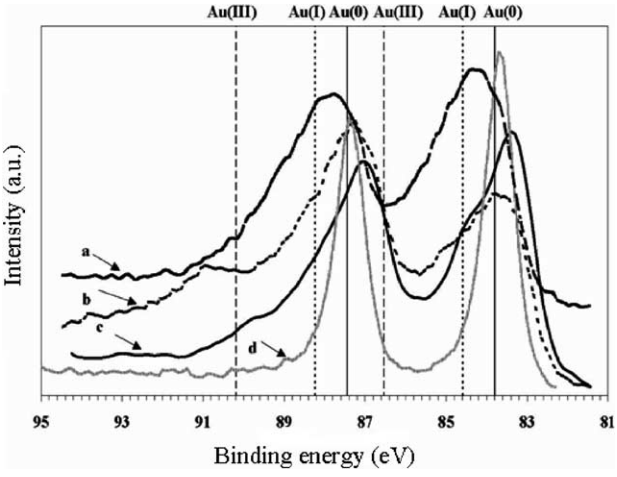

Fig. 9. XP spectra of as prepared and used 4.7Au–CL(DP); calcined at 400 °C, 10 h (see Tables 1 and 3 for properties): (a) used in 11% CO–7% CO_2–26% H_2O–26% H_2–He, in the temperature range 200–350 °C for 20 h; (b) used in 2% CO–10% H_2O–He, in the temperature range 150–350 °C for 70 h; (c) as prepared catalyst; (d) used in 5% CO–15% H_2O–35% H_2–He for 100 h; space velocity 15,000 h^{-1}; reaction temperature: 250 °C.

changed with the reaction conditions. In more oxidizing atmospheres (lines a and b) (a: 11% CO–26% H_2O–7% CO_2–26% H_2–He; b: 2% CO–10.7% H_2O–He), ionic gold is clearly seen in the used samples. However, when used in a more reducing WGS atmosphere (line d: 5% CO–15% H_2O–35% H_2–He), the peaks of Au (0) became sharper. Gold particle growth from 5.0 to 7.2 nm was measured in this sample, as can be seen in Table 3.

In previous work [13], we reported that carbon-containing species over CO-reduced ceria cannot be fully oxidized by water, although they can be removed by oxygen. Time-resolved measurements of deposition of carbon-containing species during the WGS reaction found that an initial buildup of carbon-containing species took place on the sample, but this leveled off after ~2 h, in agreement with the surface area loss [28]. Hilaire et al. [29] reported formation of carbonate species on PM–ceria under their WGS conditions. The identification of formate compounds involving geminal OH groups of ceria was recently reported by Jacobs et al. [30] on Pt–ceria. These researchers argue that the WGS reaction mechanism may involve a formate intermediate in agreement with Shido and Iwasawa [31]. Irrespective of whether this mechanism or the redox reaction mechanism [2] holds for WGS on Pt–ceria, there is a distinct possibility for carbon-containing species to form and partially block some catalyst sites.

To check this point for the gold–ceria catalysts and probe the issue of carbon deposition and regeneration, several cycles of CO-TPR followed by oxidation were carried out with one of the leached catalysts. Cyclic CO-TPR of 0.44Au–CL(DP, NaCN) is shown in Fig. 10. The same CO-TPR run was conducted four times over the sample. H_2 was produced during the CO-TPR step, by the WGS reaction, using residual surface Ce–OH groups, which were not removed in the drying and oxidative heating of the sample during preparation. The surface area only dropped 4.7%, changing from 149.8 to 142.8 m^2/g after four times of CO-TPR followed by intermittent oxidation. The CO_2 production and H_2 production during each run are shown in Table 4.

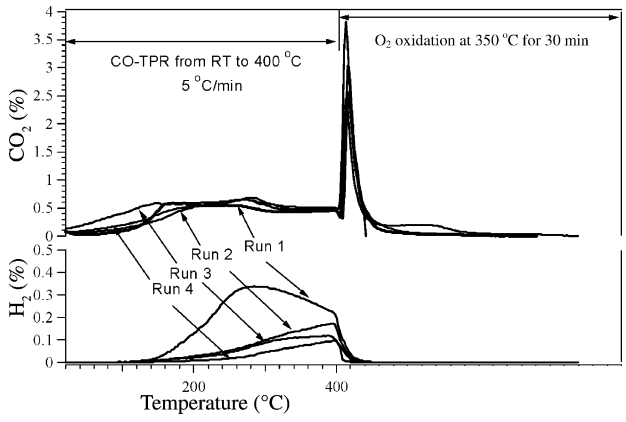

Fig. 10. Cyclic CO-TRP profiles of 0.44Au–CL(DP, NaCN). Each run was 76 min TPR + 30 min O_2 oxidation (at 350 °C) + 60 min cooling to RT in O_2; 10% CO/He; 20% O_2/He, 50 ml/min.

Table 4
CO_2 and H_2 production in cyclic CO-TPR[a]

	First run (μmol/g cat)	Second run (μmol/g cat)	Third run (μmol/g cat)	Fourth run (μmol/g cat)
CO_2 production	634.6	666.9	892.0	737.0
H_2 production	265.8	94.6	74.8	43.4

[a] Sample: 0.44Au–CL(DP, NaCN); 10% CO/He gas mixture (50 cm^3/min (NTP)), 5 °C/min to 400 °C; with intermittent reoxidation at 350 °C, 30 min (Fig. 10).

The CO_2 production in CO-TPR was almost the same in each run. H_2 was of course progressively reduced, as the OH groups of ceria were consumed with each cycle. The results shown in Fig. 10 and Table 4 demonstrate the good oxygen storage capacity of the Au–ceria sample. Furthermore, they indicate that carbonaceous species on the surface are removed by oxidation.

3.3.3. Aging tests

In a series of tests, we examined the effect of each of the gas components of the WGS reaction mixture on catalyst activity. Fig. 11 shows CO conversions measured at 300 °C in the gas mixture 11% CO–26% H_2O–26% H_2–7% CO_2–He, after 2 h exposure to each of the components of the gas mixture. A contact time of 0.25 g s/cm^3 was used in these tests. A drop in CO conversion of ~20% was observed after exposure to CO_2. Exposure to H_2O caused some transient recovery, but this was lost again with time-on-stream. Carbon monoxide exposure did not affect the subsequent performance in the reaction gas. Heating in oxygen to 350 °C at the end of the aging tests did not fully restore the catalyst activity to its initial value. The surface area of the aged catalyst at the end of this series of experiments was 109 m^2/g [28]. This is much more than the loss of surface area at 250 °C, after 100 h in the CO_2-free gas of Fig. 7. Thus, carbon dioxide causes activity and surface area losses in the gold–ceria catalyst. This is in agreement with the hypothesis of Kim and Thompson [26].

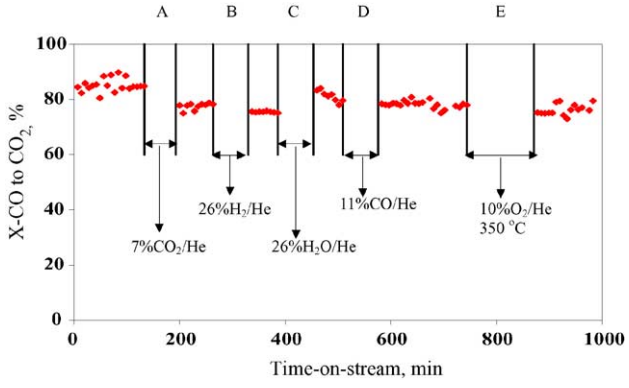

Fig. 11. Aging test of 4.7Au–CL(DP) catalyst. CO conversions were measured at 300 °C with a gas composition of 11% CO–26% H_2O–26% H_2–7% CO_2–He and contact time of 0.25g s/cm^3: (A) 300 °C in 7% CO_2–He; (B) 300 °C in 26% H_2–He; (C) 300 °C in 26% H_2O–He; (D) 300 °C in 26% H_2–He; (E) 300 °C in 10% O_2–He.

3.4. Shutdown operation

The catalyst stability under shutdown conditions was examined in this work. In fuel cell applications, the catalysts will experience frequent shutdowns and should maintain activity after exposure to reaction mixture at room temperature.

Fuel processor shutdown operation was simulated as shown in Fig. 12. The amount of 4.7Au–CL(DP) sample in this experiment was 0.84 g, the gas flow rate was maintained at 207 ml/min and the reaction temperature at 300 °C. For the first 120 min, the reaction was carried out in the gas mixture of 11% CO–26% H_2O–26% H_2–7% CO_2–He and a stable conversion of ~65% was observed. Then the sample was cooled to room temperature and held for 2 h, before it was reheated to 300 °C. The treatment was conducted in the dry gas mixture of 11% CO–26% H_2–7% CO_2–He. The CO conversion decreased to 57% after this treatment. However, a severe drop in CO conversion (to 12%) was observed when shutdown took place in the wet gas mixture of 11% CO–26% H_2–26% H_2O–7% CO_2–He by the same procedure. The surface area of the thus treated sample was only 36.4 m^2/g, which could be partially restored to 80.6 m^2/g after heating the sample in pure helium at 350 °C for 10 h. No further increase in surface area took place by oxidizing this sample in 20% O_2–He at 350 °C for 10 h. Apparently, water in conjunction with CO_2, poisons catalyst sites at ambient temperatures. XRD analysis of the gold–ceria sample as retrieved at the end of the experiment shown in Fig. 12,

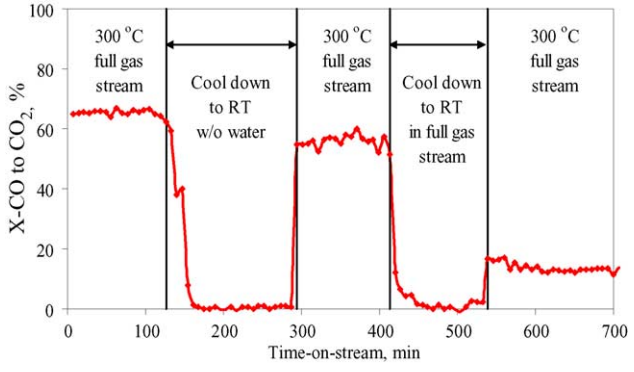

Fig. 12. Processor shutdown simulation. Catalyst: 4.7Au–CL(DP); CO conversions were measured at 300 °C in 11% CO–26% H_2O–26% H_2–7% CO_2–He; space velocity: 30,000 h^{-1}; (A) cool down to room temperature, hold for 2 h and reheat to 300 °C in the dry gas mixture of 11% CO–26% H_2–7% CO_2–He; (B) cool down to room temperature, hold for 1 h and reheat to 300 °C in the wet gas mixture of 11% CO–26% H_2O–26% H_2–7% CO_2–He.

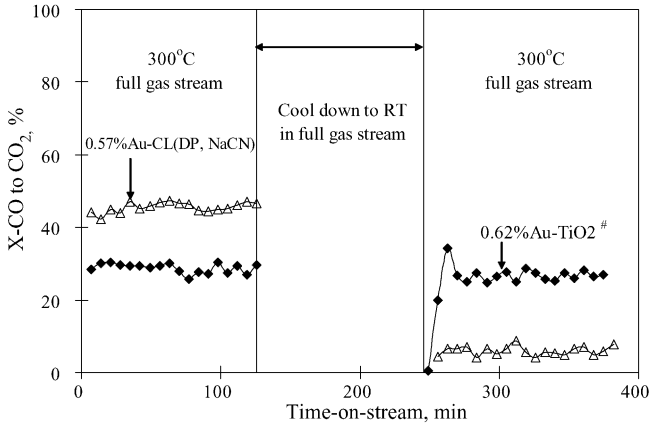

Fig. 13. Shutdown simulation using gold–ceria, 0.57 at.% Au–Ce (10% La)O_x, and gold–titania, 0.62 at.% Au/TiO_2. Gas composition: 11% CO–26% H_2O–26% H_2–7% CO_2–He; space velocity: 50,000 h^{-1}; #: World Gold Council, reference catalyst type A: 1.5 wt.% Au/TiO_2.

revealed the presence of cerium hydroxycarbonate, $CeCO_3OH$. A more detailed study is necessary to examine deactivation as a function of the water content in the gas. A potential engineering solution for stationary hydrogen generators is to divert the water flow into the heating/cooling system, and conduct shutdown in the non-condensable gas mixture only.

Fig. 13 compares the shutdown effect on the CO conversion over a 0.57 at.% Au–CL catalyst prepared by NaCN leaching from a DP-parent material not included in Table 1 [32] and the 0.62 at.% Au–TiO_2 (ref. catalyst type A, from the World Gold Council; WGS activity shown in Fig. 6). The latter shows stable activity after shutdown in the full gas mixture. However, it is inferior to the gold–ceria catalyst, as shown by its much lower steady-state CO conversion at 300 °C prior to shutdown. Efforts to stabilize the ceria surface are deemed important for the development of the next generation water–gas shift catalysts.

4. Summary/conclusions

In this work, we examined the activity and stability of Au–ceria catalysts under realistic water–gas shift reaction conditions. Metallic gold nanoparticles as well as ionic gold were found in gold–ceria catalysts. Leaching with NaCN solutions, removed all the gold species that were weakly bound on ceria. This included all the metal Au nanoparticles. The leached samples contained only a small fraction of the original amount of gold in the form of cations, apparently bound in the ceria lattice as Au–O–Ce species. Au ion substitution in ceria was suggested by a measurable lattice constant expansion of the crystal.

Similar rates of CO_2 production by the water gas shift reaction were measured over the parent and leached gold–ceria catalysts. The extra gold present in the parent material does not increase the rate; nor does it change the activation energy of the reaction. Reaction rates scale with the amount of gold present in the leached samples. They also scale with the amount of gold present in low-content gold–ceria samples prepared by single-pot UGC synthesis. These findings hold true for undoped ceria as well as for La- or Gd-doped nanocrystalline cerias.

The number of active sites was found to correlate well with the properties of the support oxide, namely the ceria surface area and crystallite size. For the Au–ceria catalysts prepared by DP, the smaller the crystallite size of ceria, the larger the amount of gold retained after leaching. Large-sized ceria particles produced by annealing at 800 °C did not retain any gold after leaching. The method of preparation affects the catalyst properties. Gelation or coprecipitation techniques can be suitably developed to prepare a catalyst with a large concentration of active sites.

Gold–ceria catalysts are stable at low-temperature WGS reaction conditions. Through strong interaction with the Ce–O species, gold ions are stabilized in the ceria matrix. Furthermore, the incorporation of Au into ceria can suppress the sintering of ceria at temperatures as high as 800 °C. Initial loss of activity under reaction conditions is small, and correlates well with a concomitant loss of ceria surface area in the reaction mixture. Gas composition plays an important role in controlling the oxidation state of gold, but this is a complex function of the gas composition–temperature effect on the ceria surface reduction/oxidation. Shutdown operation in the full gas stream has identified a stability problem due to cerium oxide—hydroxycarbonate formation. This needs to be properly addressed.

A general conclusion from this work is that the active sites for the WGS reaction on gold–ceria and potentially other Au-oxide systems, as well as other metals on ceria [6] are nonmetallic. Phases involving metal cations and the oxide support, M–O–Ce, appear to do the catalysis. Whether this holds true for other oxidation reactions on oxide-supported metals is worth pursuing in future work. This opens the field to new catalyst designs involving metal ions in oxide supports, and potentially new cost-effective catalyst solutions to meet the needs of the hydrogen economy in the near future.

Acknowledgement

The financial support of this work by the NSF/EPA, Grant No. CTS-9985305 and by the NSF Nanotechnology Interdisciplinary Research Team (NIRT) Grant No. 0304515, is gratefully acknowledged.

References

[1] D.S. Newsome, Catal. Rev. Sci. Eng. 21 (1980) 275.
[2] T. Bunluesin, R.J. Gorte, G.W. Graham, Appl. Catal. B 15 (1998) 107.

[3] S. Hilaire, X. Wang, T. Luo, R.J. Gorte, J. Wagner, Appl. Catal. A: Gen. 215 (2001) 271.
[4] S.L. Swartz, M.M. Seabaugh, C.T. Holt, W.J. Dawson, Fuel Cell Bull. 30 (2001) 7.
[5] Y. Li, Q. Fu, M. Flytzani-Stephanopoulos, Appl. Catal. B 27 (2000) 179.
[6] Q. Fu, H. Saltsburg, M. Flytzani-Stephanopoulos, Science 301 (2003) 935, published online 3 July (10.1126/science.1085721).
[7] A. Trovarelli (Ed.), Catalysis by Ceria and Related Materials, Catalytic Science Series, vol. 2, Imperial College Press, London, 2002.
[8] T. Zhu, L. Kundakovic, A. Dreher, M. Flytzani-Stephanopoulos, Catal. Today 50 (2) (1999) 381.
[9] L. Kundakovic, M. Flytzani-Stephanopoulos, J. Catal. 179 (1998) 203.
[10] W. Liu, M. Flytzani-Stephanopoulos, J. Catal. 153 (1995) 304.
[11] W. Liu, M. Flytzani-Stephanopoulos, J. Catal. 153 (1995) 317.
[12] Q. Fu, A. Weber, M. Flytzani-Stephanopoulos, Catal. Lett. 77 (1–3) (2001) 87.
[13] Q. Fu, S. Kudriavtseva, H. Saltsburg, M. Flytzani-Stephanopoulos, Chem. Eng. J. 93 (2003) 41.
[14] H.C. Yao, Y.F. Yu Yao, J. Catal. 86 (1984) 254.
[15] S. Gardner, G. Hoflund, D. Schryer, J. Schryer, B. Upchurch, E. Kielin, Langmuir 7 (1991) 2135.
[16] D. Andreeva, V. Idakiev, T. Tabakova, L. Ilieva, P. Falaras, A. Bourlinos, A. Travlos, Catal. Today 72 (1–2) (2002) 51.
[17] M. Haruta, N. Yamada, T. Kobayashi, S. Iijima, J. Catal. 115 (1989) 301.
[18] M. Valden, X. Lai, D.W. Goodman, Science 281 (1998) 1647.
[19] G.C. Bond, D.T. Thompson, Gold Bull. 33 (2) (2000) 41.
[20] N. Hedley, H. Tabachnik, Chemistry of Cyanidation, American Cyanamid Company, Wayne, NJ, 1968.
[21] L. Minervini, M.O. Zacate, R.W. Grimes, Solid State Ionics 116 (1999) 339.
[22] F. Zhang, S.-W. Chan, J.E. Spanier, E. Apak, Q. Jin, R.D. Robinson, I.P. Herman, Appl. Phys. Lett. 80 (1) (2002) 127.
[23] J.M. Zalc, V. Sokolovskii, D.G. Loffler, J. Catal. 206 (2002) 169.
[24] F. Ghenciu, Curr. Opin. Solid State Mater. Sci. 6 (5) (2002) 389.
[25] X. Wang, R.J. Gorte, J.P. Wagner, J. Catal. 212 (2002) 225.
[26] C.H. Kim, L. Thompson, Preprints Symp. ACS, Div. Fuel Chem. 48 (1) (2003) 233.
[27] J. Guzman, B.C. Gates, J. Phys. Chem. B 107 (2003) 2242.
[28] Q. Fu, Ph.D. Dissertation, Department of Chemical and Biological Engineering, Tufts University, Medford, MA, 2004.
[29] S. Hilaire, X. Wang, T. Luo, R.J. Gorte, J. Wagner, Appl. Catal. A: Gen. 215 (2001) 271.
[30] G. Jacobs, L. Williams, U. Graham, G.A. Thomas, D.E. Sparks, B.H. Davis, Appl. Catal. A: Gen. 252 (2003) 107.
[31] T. Shido, Y. Iwasawa, J. Catal. 141 (1993) 71.
[32] W. Deng, Ph.D. Thesis, Tufts University, in preparation.